ICCES, 2023, vol.27, no.3
DOI: 10.32604/icces.2023.010442

PROCEEDINGS

How Travelling Wavelength Affects Hydrodynamic Performance of Two Linear-Accelerating Mirror-Symmetric Fish-Like Swimmers

Zhonglu Lin[1,2], Dongfang Liang[2] and Yu Zhang[1,*]

[1] Key Laboratory of Underwater Acoustic Communication and Marine Information Technology of the Ministry of Education, College of Ocean and Earth Sciences, Xiamen University, Xiamen, 361102, China

[2] Cambridge University Engineering Department, Trumpington St, Cambridge, CB2 1PZ, UK

[*] Corresponding Author: Yu Zhang. Email: yuzhang@xmu.edu.cn

ABSTRACT

Fish schools are capable of simultaneous linear acceleration. To reveal the underlying hydrodynamic mechanism, we numerically investigate how Reynolds number Re = 1000–2000, Strouhal number St = 0.2–0.7 and wavelength λ = 0.5–2 affects the mean net thrust of two side-by-side NACA0012 hydrofoils undulating in anti-phase. In total, 550 cases are simulated using immersed boundary method. The thrust is strengthened by wavelength and Strouhal number, yet only slightly by the Reynolds number. We apply the symbolic regression algorithm to formulate this relationship as a high-level summary.

KEYWORDS

Fish swimming; linear acceleration; immersed boundary method; biomimetic hydrodynamics

1 Introduction

Fish swimming and schooling have been extensively studied for decades [1, 2, 3] from various disciplines, e.g. anatomy [2], animal behaviour [4], robotics [5], simulation [6, 7], etc. In the nature, fish swimming body wavelength is not only different across various species with different swimming styles [8], but also differs with the locomotion phase of a single swimmer [9], e.g. starting from rest, linear acceleration and steady swimming. Santo et al. [8] recently conducted a comparative study on the kinematics of 44 BCF fish species, focusing on the steady swimming phase. An overview of the wavelength and swimming styles is demonstrated in Figure 1. Santo et al. [8] summarised and compared the wavelengths of different BCF species, considering the four classic swimming styles of *anguilliform*, *subcarangiform*, *carangiform* and *thunniform*. The median wavelength significantly increased from *anguilliform* (0.75 Body Length) to *thunniform* (1.14 Body Length), yet the wavelength for their tested species occupies a broader range from 0.5 Body Length to 1.5 Body Length. In the following content, we abbreviate "body length" as "BL" for conciseness. Du Clos et al. [9] studied how an *anguilliform* swimmer, *Petromyzon marinus*, accelerates from rest, comparing the kinematics during steady swimming and acceleration. They discovered that the wavelength during escape acceleration $\lambda \approx 2$ could be much longer than that during steady swimming $\lambda = 0.8$.

Many numerical studies also focused on the wavelength effect of a single swimmer, both in 2D and 3D. Chao et al. [10] recently investigated the hydrodynamic performance of a single slender swimmer with various Strouhal numbers $St = 0.1{-}1$, Reynolds number $Re = 50{-}2000$, and $\lambda = 0.5{-}2$, discovering seven types of wake structures. They were able to condense the simulation results into a few formulas. Their study has inspired the present study's choice of parametric space. Khalid et al. [11] studied how a single tethered undulating 2D NACA0012 hydrofoil swims with either *anguilliform* or *carangiform* kinematics in a parametric sweep of $Re = 100, 1000, 5000$, $St = 0.1{-}0.8$, and $\lambda = 0.5{-}1.5$. Thekkethil et al. [12, 13, 14]

conducted a series of studies regarding how the wavelength affects the thrust of a single undulating NACA0012 hydrofoil. Carling et al. [16] investigated a free-swimming 2D *anguilliform* swimmer with a constant wavelength $\lambda = 1$.

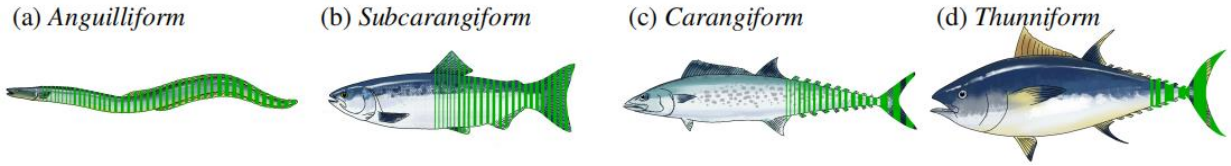

Figure 1: Four different swimming modes of Body-Caudal-Fin type locomotion (a) *Anguilliform* (body undulation, e.g. eel) (b) *Subcarangiform* (body undulation with caudal fin pitching, e.g. salmonid) (c) *Carangiform* (minor body undulation with caudal fin pitching, e.g. makrell) (d) *Thunniform* (mainly caudal fin pitching, e.g. tuna).

The shaded area demonstrates the body parts with a significant lateral motion to generate thrust (redrawn from figures by [23] and [24]). These four types have wavelengths ranging from 0.5BL to 2BL for steady swimming conditions across various fish species regardless of the BCF sub-types [8].

Wavelength correlates significantly with acceleration and speed during the linear acceleration phase of fish swimming. The existing biological research almost all focused on a single accelerating fish. Schwalbe et al. [17] scrutinised the function of red muscle during the acceleration of bluegill sunfish *Lepomis macrochirus* and how it affects fish kinematics. They discovered that the fish's undulation kinematics during acceleration differs from that during steady swimming. Body wavelength decreases significantly during acceleration, yet increases significantly with swimming speed. Their research focused on the bluegill sunfish *Lepomis macrochirus*; during the different acceleration levels, the fish body wavelength can range from 0.75BL to 0.9BL. They focused on the fish muscle activation and observation of kinematics. Akanyeti et al. [18] conducted biological and robotic fish experiments to investigate the kinematic characteristics and hydrodynamic performance during linear acceleration. Their investigation was carried out using a tethered robotic fish while varying the free stream flow to study the acceleration at consecutive instants. Our present problem setup is consistent with their experimental configuration. They found that tail-beat frequency is most effective on swimming speed and acceleration. However, the tail-beat amplitude remains constant during steady swimming or acceleration. So the present study fixed tail-beat amplitude while varying the Strouhal number.

Side-by-side fish schooling is relatively well studied, yet most studies have focused on the steady swimming scenario with fixed wavelength. Ashraf et al. [4] conducted a fish schooling experiment, discovering that fish favours the phalanx formation, i.e. side-by-side of multiple fish, at relatively high steady-swimming speed. The tested Reynolds number ranges from 1000 to 6000. Li et al. [19] investigated the schooling of two robotic fish of *subcarangiform*, swimming steadily side-by-side with rigid linking between them; the lateral distance is fixed at 0.33BL. For schooling swimmers, they discovered maximum speed and efficiency at in-phase and anti-phase conditions, respectively, compared with a single swimmer. In the present paper, we also chose to fix the gap distance at 0.33BL. In many studies, NACA hydrofoils have been used as representative swimmer geometry. Deng et al. [20, 21] studied the energy extraction performance of a flapping foil using NACA0015. Deng et al. [22] conducted a numerical study to examine the propulsive efficiency of a heaving and flapping NACA0012 foil at a Reynolds number of $Re = 1700$.

In summary, although excellent studies have emerged for single fish wavelength effects, linear acceleration and side-by-side schooling, yet how fish body wavelength affects the linear acceleration of two side-by-side fishlike swimmers remains a question. We aim to answer this question in the present paper.

2 Methodology

In this section, we present the methodology of the current study. First, section 2.1 describes the representative problem setup accounting for the schooling swimmers, including geometry, kinematic

equation, and non-dimensional analysis. Then, section 2.2 discusses the computational method applied to implement the problem setup.

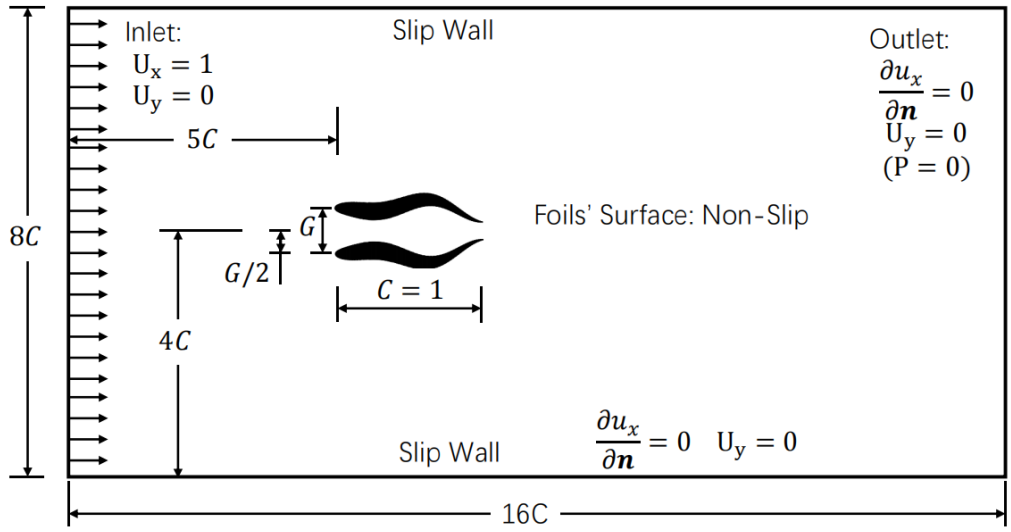

Figure 2: Sketch of the present problem setup: two side-by-side fish swimming in anti-phase with a fixed lateral gap distance G = 0.33. The two swimmers are mirror symmetric to each other along the horizontal line $y = 4C$ at any instant.

2.1 Problem setup

The current problem setup can be summarised in Figure 2. The accelerated fish schooling problem is represented by a two-dimensional form with two wavy hydrofoils undulating side-by-side. The 2D configuration should adequately describe the present laminar flow regime with $Re \leq 2000$ [25, 10].

The fish body is simplified as a 2D NACA0012 hydrofoil, which has been widely used to describe bio-propulsion problems with pitching [26] and undulating hydrofoils [12]. The geometry of a NACA0012 hydrofoil can be similar to that of a *carangiform* or *subcarangiform* swimmer. The two foils are placed side-by-side while undulating in anti-phase to concentrate on a limited number of variables typical for fish schooling [4]. The kinematics of the swimmers are described by the travelling wave equations in the nondimensional form:

$$Y_1 = A_{max} X_1 \sin\left[2\pi\left(\frac{X_1}{\lambda} - \frac{St}{2A_{max}}t\right)\right] \tag{1}$$

$$Y_2 = A_{max} X_2 \sin\left[2\pi\left(\frac{X_2}{\lambda} - \frac{St}{2A_{max}}t\right) + \pi\right] \tag{2}$$

This is also a common configuration [13], chosen here for the convenience of comparison. For completeness, the meaning of the variables is listed as follows: $Y_i = Y_i'/C'$ is the centre-line lateral displacement of each hydrofoil; $X_i = X_i'/C'$ is the streamwise position on the centre-line; i = 1 denotes the top swimmer while i = 2 represents the bottom swimmer. $t = t'u_\infty'/C'$ is non-dimensional time; u_∞' is the freestream velocity; $A_{max} = A_{max}'/C'$ is non-dimensional tail tip amplitude, where C' is the fish body length; A_{max}' is the dimensional tail-amplitude; $\lambda = \lambda'/C'$ is the non-dimensional wavelength, with λ' being the dimensional foil undulating wavelength; $St = 2f'A_{max}'/u_\infty'$ is Strouhal number, with f' being the dimensional undulating frequency. Here, the dashed alphabets denote the dimensional parameters.

In addition, the non-dimensional groups to describe a particular case are listed in Table 1 together with the investigated parametric space, where ρ' is the fluid density; f' is the undulating frequency. In summary, only three variables are involved in the present study: Reynolds number Re = 1000−2000, Strouhal number St = 0.2−0.7, and non-dimensional wavelength λ = 0.5−2.0. The thrust is directly relevant to the acceleration. Cycle-averaged net thrust coefficient $\bar{C}_{T,i}$ is defined as $\frac{1}{T}\int_t^{t+T} C_T dt = \frac{1}{T}\int_t^{t+T} 2F_{T,i} / \rho u_\infty^2 C dt$, where $F_{T,i}$ is the net thrust on hydrofoils.

Table 1: Non-dimensional input parameters and the involved range of value

Reynolds number	Re	$\rho u_\infty C/\mu$	$1000-2000$
Strouhal number	St	$2fa_{max}/u_\infty$	$0.2-0.7$
Wavelength	λ	λ'/C	$0.5-2$

2.2 Computational method

The present paper simulates the problem using a customised version of the ConstraintIB module [27, 28] among the IBAMR [29], which is an open-source immersed boundary method simulation software that depends on several underlying advanced libraries, including SAMRAI [30, 31], PETSc [32, 33, 34], hypre [35, 32], and libmesh [36]. The ConstraintIB has been extensively validated [27, 37, 38, 28], and the present customised version has also been validated [39]. The Reynolds number $Re \leq 2000$ in the present study is lower than that in a previous study [39] with Re = 5000, so here, we adopt the same mesh setting that has been verified for mesh independence.

3 How *St*, λ and *Re* affect net thrust $\bar{C}_{T,pair}$

This section discusses how the net propulsive efficiency varies with Reynolds number Re = 1000 − 2000, Strouhal number St = 0.2−0.7, and wavelength λ = 0.5−2. The thrust generally increases with Strouhal number and wavelength, whereas the effect of Reynolds number is marginal, as demonstrated in Figure 3. The contour line of $\bar{C}_{T,pair}$ = 0 at the white region denotes the condition corresponding to the steady swimming state, which is often discussed in numerical [40] and experimental [5] studies of fish swimming. With a higher St or λ, the thrust becomes positive $\bar{C}_{T,pair} > 0$, i.e. the swimmer school accelerates. Conversely, with a lower St or λ, the foils are decelerating with negative thrust. Re only slightly affects this overall trend. This pattern corresponds well with the single swimmer scenario discussed in [10], where the effect of Re for net thrust becomes insignificant at $Re > 1000$ while a positive correlation exists between net thrust and wavelength/Strouhal number.

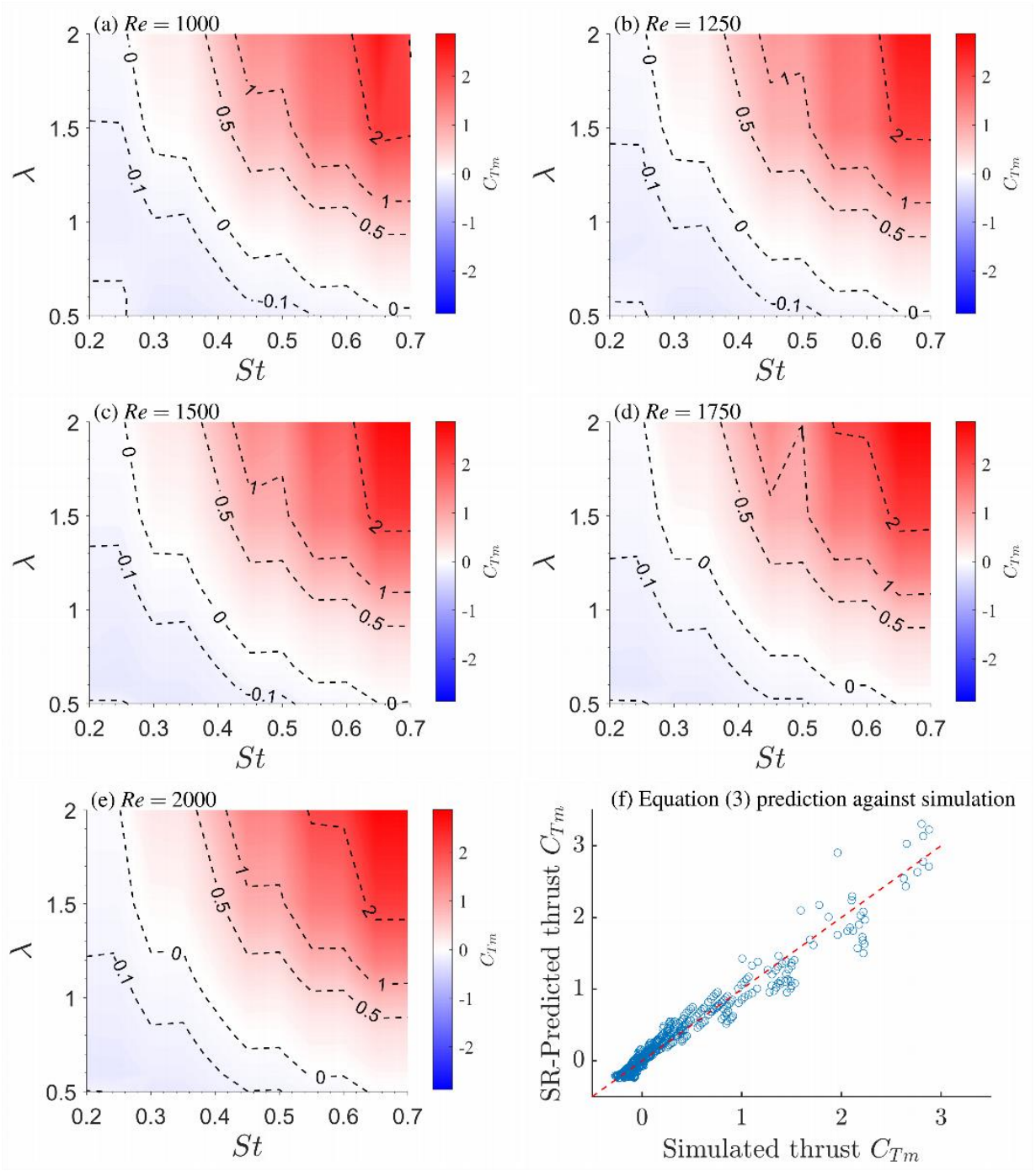

Figure 3: Heat map for mean net thrust $\bar{C}_{T,pair}$ at Strouhal number St = 0.2−0.7, wavelength λ = 0.5−2 and Reynolds numbers at (a) Re = 1000 (b) Re = 1250 (c) Re = 1500 (d) Re = 1750 (e) Re = 2000. (f) Symbolic regression prediction accuracy comparing simulation results and Equation (3). The thrust on the two swimmers is identical due to the symmetrical situation. The positive thrust, i.e. forward acceleration, is indicated by the positive values with red colour. Conversely, the negative thrust, i.e. deceleration, is indicated by the negative values with blue colour. The contour line of $\bar{C}_{T,pair}$ = 0 represents the zero net thrust scenarios, i.e. steady swimming state. Only marginal differences can be observed across various Reynolds numbers.

Here, we offer a high-level summary of the mean net thrust $\bar{C}_{T,pair}$ of the side-by-side and anti-phase scenarios. Following the formalities of previous studies regarding a flapping foil [41, 42, 43] and an undulating foil [10], we use the symbolic regression tool PySR [44, 45] to automatically produce an interpretable equation that summarises the $\bar{C}_{T,pair}$ data in the present study for schooling swimmers, as seen in Equation (3):

$$\bar{C}_{T,pair} = Re^{0.17} St^{2.03} \lambda^{1.23} - 0.26 Re^{0.19} St^{1.00} \lambda^{0.10} - 6.13 Re^{-0.6} \tag{3}$$

The summarising capability of Equation (3) can be demonstrated in Figure 3f. For the convenience of the readers' comparison, here we also copy the $\bar{C}_{T,pair}$ equation by [10] for a single swimmer as Equation (4):

$$\bar{C}_{T,single} = 0.36 Re^{0.208} St^{3} \lambda - 6.13 Re^{-0.6} \tag{4}$$

We can see that compared with the single swimmer thrust $\bar{C}_{T,single}$ formula produced by [10], the additional mirror-symmetric swimmer cast an interesting effect on the $\bar{C}_{T,pair}$ of each schooling member. Wavelength scales with net thrust as $\bar{C}_{T,pair} \sim \lambda^{1.23}$ when the Strouhal number *St* and wavelength are relatively small. The scaling component at schooling condition is slightly higher than single swimmer scenarios $\bar{C}_{T,single} \sim \lambda^{1}$, indicating the wavelength can be more influential to the net thrust at schooling condition. On the other λ hand, the primary scaling of $\bar{C}_{T,pair}$ with Strouhal number is reduced from $\bar{C}_{T,pair} \sim St^{3}$ for a single foil [10] to $\bar{C}_{T,pair} \sim St^{2.03}$ in Equation (3), so the contribution from the Strouhal number to net thrust becomes less significant for the anti-phase schooling scenario compared with the single swimmer case. In contrast, the scaling exponent of 2.03 in Equation (3) is very close to that of two side-by-side pitching foils, i.e. at λ=+∞, which scale as $\bar{C}_{T,pair} \sim St^{2}$ [46].

4 Conclusions

The effects of fish body wavelength on its linear acceleration during side-by-side schooling conditions seems never studied in detail. In the present paper, we conducted a systematic simulation study for 550 cases of two linearly-accelerating side-by-side wavy NACA0012 hydrofoils swimming in anti-phase. We examined the net thrust distribution by drawing heat maps and generating summarising formulas. The simulation is conducted on a customised version of the ConstraintIB [27, 28] module from the IBAMR [29] open-source library. The parametric space is tested for Strouhal number St = 0.2−0.7, wavelength λ= 0.5−2 and Reynolds number Re = 1000−2000. In contrast, lateral gap distance and maximum tail amplitude are fixed at G = 0.33 and A_{max} = 0.1. This range is chosen based on BCF swimmers in the nature [25, 8].

In the present paper, we propose an equation as a high-level summary for the mean net thrust on each undulating swimmer: $\bar{C}_{T,pair} = Re^{0.17} St^{2.03} \lambda^{1.23} - 0.26 Re^{0.19} St^{1.00} \lambda^{0.10} - 6.13 Re^{-0.6}$. Mean net thrust increases with wavelength λ and Strouhal number *St*, yet only slightly with Reynolds number *Re*. When the λ and *St* are relatively small, the thrust increases almost linearly with wavelength $\bar{C}_{T,pair} \sim \lambda^{1.23}$ while scaling with Strouhal number as $\bar{C}_{T,pair} \sim St^{2}$, rather than $\bar{C}_{T,pair} \sim St^{3}$ for a single swimmer [10].

In the future, we will continue to study the wavelength effects on propulsive efficiency and the enhancement of thrust and efficiency from swimming alone to schooling condition.

Funding Statement: This work was funded by China Postdoctoral Science Foundation under Grant Number 2021M691865. This work was also financially supported by the Project supported by the National Natural Science Foundation of China (Grant Nos. 12074323; 42106181), the Science and Technology

Major Project of Fujian Province (Grant Nos. 2021NZ033016), the Natural Science Foundation of Fujian Province of China (No.2022J02003), the China National Postdoctoral Program for Innovative Talents (Grant No. BX2021168) and the Outstanding Postdoctoral Scholarship, State Key Laboratory of Marine Environmental Science at Xiamen University.

Conflicts of Interest: The authors declare that they have no conflicts of interest to report regarding the present study.

References

1. Webb, P. W. (1984). Form and Function in Fish Swimming. *Scientific American, 251(1).*
2. Weihs, D. (1973). Hydromechanics of Fish Schooling. *Nature, 241(5387),* 290–291.
3. Chao, L. M., Alam, M. M., Ji, C. (2021). Drag-thrust transition and wake structures of a pitching foil undergoing asymmetric oscillation. *Journal of Fluids and Structures, 103*.
4. Ashraf, I., Bradshaw, H., Ha, T. T., Halloy, J., Godoy-Diana, R., et al. (2017). Simple phalanx pattern leads to energy saving in cohesive fish schooling. *Proceedings of the National Academy of Sciences of the United States of America, 114(36),* 9599-9604.
5. Li, L., Nagy, M., Graving, J. M., Bak-Coleman, J., Xie, G., et al. (2020). Vortex phase matching as a strategy for schooling in robots and in fish. *Nature Communications. 11,* 5408.
6. Borazjani, I., Sotiropoulos, F. (2010). On the role of form and kinematics on the hydrodynamics of self-propelled body/caudal fin swimming. *Journal of Experimental Biology, 213(1),* 89–107.
7. Chao, L. M., Pan, G., Zhang, D., Yan, G. X. (2019). On the two staggered swimming fish. Chaos, *Solitons and Fractals, 123,* 260-262.
8. Santo, V. D., Goerig, E., Wainwright, D. K., Akanyeti, O., Liao, J. C., et al. (2021). Convergence of undulatory swimming kinematics across a diversity of fishes. *Proceedings of the National Academy of Sciences of the United States of America, 118(49),* e2113206118.
9. Du Clos, K. T., Dabiri, J. O., Costello, J. H., Colin, S. P., Morgan, J. R., et al. (2019). Thrust generation during steady swimming and acceleration from rest in anguilliform swimmers. *Journal of Experimental Biology, 222(22),* jeb212464.
10. Chao, L.-M., Alam, M. M., Cheng, L. (2022). Hydrodynamic performance of slender swimmer: effect of travelling wavelength. *Journal of Fluid Mechanics, 94,* A8.
11. Khalid, M. S. U., Wang, J., Dong, H., Liu, M. (2020). Flow transitions and mapping for undulating swimmers. *Physical Review Fluids, 5,* 063104.
12. Thekkethil, N., Shrivastava, M., Agrawal, A., Sharma, A. (2017). Effect of wavelength of fish-like undulation of a hydrofoil in a free-stream flow. *Sadhana - Academy Proceedings in Engineering Sciences, 42(4),* 585-595.
13. Thekkethil, N., Sharma, A., Agrawal, A. (2018). Unified hydrodynamics study for various types of fishes-like undulating rigid hydrofoil in a free stream flow. *Physics of Fluids, 30,* 077107.
14. Thekkethil, N., Sharma, A., Agrawal, A. (2020). Self-propulsion of fishes-like undulating hydrofoil: A unified kinematics based unsteady hydrodynamics study. *Journal of Fluids and Structures, 93,* 102875.
15. Gupta, S., Thekkethil, N., Agrawal, A., Hourigan, K., Thompson, M. C., et al. (2021). Body-caudal fin fish-inspired self-propulsion study on burst-and-coast and continuous swimming of a hydrofoil model. *Physics of Fluids, 33,* 091905.
16. Carling, J., Williams, T. L., Bowtell, G. (1998). Self-propelled anguilliform swimming: Simultaneous solution of the two-dimensional Navier-Stokes equations and Newton's laws of motion. *Journal of Experimental Biology, 201(23),* 3143–3166.
17. Schwalbe, M. A., Boden, A. L., Wise, T. N., Tytell, E. D. (2019). Red muscle activity in bluegill sunfish Lepomis macrochirus during forward accelerations. *Scientific Reports, 9,* 8088.
18. Akanyeti, O., Putney, J., Yanagitsuru, Y. R., Lauder, G. V., Stewart, W. J., et al. (2017). Accelerating fishes increase propulsive efficiency by modulating vortex ring geometry. *Proceedings of the National Academy of*

Sciences of the United States of America, 114(52), 13828-13833.

19. Li, L., Ravi, S., Xie, G., Couzin, I. D. (2021). Using a robotic platform to study the influence of relative tailbeat phase on the energetic costs of side-by-side swimming in fish. *Proceedings of the Royal Society A: Mathematical, Physical and Engineering Sciences, 477(2249)*, 20200810.
20. Deng, J., Wang, S., Kandel, P., Teng, L. (2022). Effects of free surface on a flapping-foil based ocean current energy extractor. *Renewable Energy, 181*, 933-944.
21. Deng, J., Teng, L., Pan, D., Shao, X. (2015). Inertial effects of the semi-passive flapping foil on its energy extraction efficiency. *Physics of Fluids, 27*, 053103.
22. Deng, J., Sun, L., Lubao Teng, Pan, D., Shao, X. (2016). The correlation between wake transition and propulsive efficiency of a flapping foil: A numerical study. *Physics of Fluids, 28*, 094101.
23. Lindsey, C. C. (1978). Form, function, and locomotory habits in fish. *Fish Physiology, 7(1978)*, 1-100.
24. Sfakiotakis, M., Lane, D. M., Davies, J. B. C. (1999). Review of fish swimming modes for aquatic locomotion. *IEEE Journal of Oceanic Engineering, 24(2)*, 237-252.
25. Gazzola, M., Argentina, M., Mahadevan, L. (2014). Scaling macroscopic aquatic locomotion. *Nature Physics, 10*, 758-761.
26. Moriche, M., Flores, O., García-Villalba, M. (2016). Three-dimensional instabilities in the wake of a flapping wing at low Reynolds number. International Journal of Heat and Fluid Flow, *62, Part A*, 44-55.
27. Bhalla, A. P. S., Bale, R., Griffith, B. E., Patankar, N. A. (2013). A unified mathematical framework and an adaptive numerical method for fluid-structure interaction with rigid, deforming, and elastic bodies. *Journal of Computational Physics, 250*, 446-476.
28. Griffith, B. E., Patankar, N. A. (2020). Immersed Methods for Fluid-Structure Interaction. *International Journal of Heat and Fluid Flow, 75*, 301-309.
29. Griffith, B. E. (2013). IBAMR: An adaptive and distributed-memory parallel implementation of the immersed boundary method. https://ibamr. github. io/about.
30. Hornung, R. D., Kohn, S. R. (2002). Managing application complexity in the SAMRAI object-oriented framework. *Concurrency and Computation: Practice and Experience, 14(5)*, 347-368.
31. Hornung, R. D., Wissink, A. M., Kohn, S. R. (2006). Managing complex data and geometry in parallel structured AMR applications. *Engineering with Computers, 22(3-4)*, 181-195.
32. Balay, S., Gropp, W. D., McInnes, L. C., Smith, B. F. (1997). Efficient Management of Parallelism in Object-Oriented Numerical Software Libraries. *Modern Software Tools for Scientific Computing*, 163-202.
33. Balay, S., Buschelman, K., Eijkhout, V., Gropp, W., Kaushik, D., et al. (2010). PETSc Users Manual. *ReVision, 2(March)*.
34. Balay, S., Abhyankar, S., Adams, M. F., Brown, J., Brune, P., et al. (2001). PETSc web page, https://petsc.org/.
35. Falgout, R., Cleary, A., Jones, J., Chow, E., Henson, V., et al. (2010). HYPRE: High Performance Preconditioners. *Users Manual. Version, 1*.
36. Kirk, B. S., Peterson, J. W., Stogner, R. H., Carey, G. F. (2006). libMesh : a C++ library for parallel adaptive mesh refinement/coarsening simulations. *Engineering with Computers, 22(3-4)*, 237–254.
37. Nangia, N., Johansen, H., Patankar, N. A., Bhalla, A. P. S. (2017). A moving control volume approach to computing hydrodynamic forces and torques on immersed bodies. *Journal of Computational Physics, 347*, 437-462.
38. Nangia, N., Patankar, N. A., Bhalla, A. P. S. (2019). A DLM immersed boundary method based wavestructure interaction solver for high density ratio multiphase flows. *Journal of Computational Physics, 398*, 108804.
39. Lin, Z., Bhalla, A. P. S., Griffith, B. E., Sheng, Z., Li, H., et al. (2023). How swimming style and schooling affect the hydrodynamics of two accelerating wavy hydrofoils. *Ocean Engineering, 268*, 113314.
40. Borazjani, I., Sotiropoulos, F. (2008). Numerical investigation of the hydrodynamics of carangiform swimming in the transitional and inertial flow regimes. *Journal of Experimental Biology, 211(10)*, 1541–1558.
41. Floryan, D., Van Buren, T., Rowley, C. W., Smits, A. J. (2017). Scaling the propulsive performance of heaving and pitching foils. *Journal of Fluid Mechanics, 822*, 386-397.
42. Van Buren, T., Floryan, D., Quinn, D., Smits, A. J. (2017). Nonsinusoidal gaits for unsteady propulsion. *Physical*

Review Fluids, 2, 053101.

43. Alam, M. M., Muhammad, Z. (2020). Dynamics of flow around a pitching hydrofoil. *Journal of Fluids and Structures, 99,* 103151.
44. Cranmer, M. (2020). PySR: Fast & Parallelized Symbolic Regression in Python/Julia. http://doi.org/10.5281/zenodo.4041459.
45. Cranmer, M., Sanchez-Gonzalez, A., Battaglia, P., Xu, R., Cranmer, K., et al. (2020). Discovering Symbolic Models from Deep Learning with Inductive Biases. arXiv:2006. 11287v2.
46. Gungor, A., Hemmati, A. (2021). The scaling and performance of side-by-side pitching hydrofoils. *Journal of Fluids and Structures, 104,* 103320.